



# 1 Influence of acidity on liquid–liquid phase transitions of mixed SOA 2 proxy–inorganic aerosol droplets

3 Yueling Chen<sup>1</sup>& Xiangyu Pei<sup>1</sup>, Huichao Liu<sup>1</sup>, Yikan Meng<sup>1</sup>, Zhengning Xu<sup>1</sup>, Fei Zhang<sup>1</sup>, Chun Xiong<sup>1</sup>,  
4 Thomas C. Preston<sup>3</sup>, Zhibin Wang<sup>1,2,4\*</sup>

5 <sup>1</sup>College of Environmental and Resource Sciences, Zhejiang Provincial Key Laboratory of Organic Pollution Process and  
6 Control, Zhejiang University, Hangzhou 310058, China

7 <sup>2</sup>ZJU-Hangzhou Global Scientific and Technological Innovation Center, Zhejiang University, Hangzhou 311215, China

8 <sup>3</sup>Department of Atmospheric and Oceanic Sciences and Department of Chemistry, McGill University, 805 Sherbrooke Street  
9 West, Montreal, Quebec H3A 0B9, Canada

10 <sup>4</sup>Key Laboratory of Environment Remediation and Ecological Health, Ministry of Education, Zhejiang University, Hangzhou  
11 310058, China

12 *Correspondence to:* Zhibin Wang ([wangzhibin@zju.edu.cn](mailto:wangzhibin@zju.edu.cn))

13 Yueling Chen and Xiangyu Pei contribute equally to this work.

14 **Abstract.** Phase state and morphology of aerosol particles play a critical role in determining their effect on climate. While  
15 aerosol acidity has been identified as a key factor affecting the multiphase chemistry and phase transitions, the impact of  
16 acidity on phase transition of multicomponent aerosol particles has not been extensively studied in situ. In this work, we  
17 employ an aerosol optical tweezer (AOT) to probe the impact of acidity on the phase transition behavior of levitated aerosol  
18 particles. Our results reveal that higher acidity decreases the separation relative humidity (SRH) of aerosol droplets mixed with  
19 ammonium sulfate (AS) and secondary organic aerosol (SOA) proxy, such as 3-methylglutaric acid (3-MGA), 1,2,6-  
20 hexanetriol (HEXT) and 2,5-hexanediol (HEXD) across aerosol pH in atmospheric condition. Phase separation of organic  
21 acids was more sensitive to acidity compared to organic alcohols. We found the mixing relative humidity (MRH) was  
22 consistently higher than the SRH in several systems. Phase-separating systems, including 3-MGA/AS, HEXT/AS, and  
23 HEXD/AS, exhibited oxygen-to-carbon ratios (O:C) of 0.67, 0.50, and 0.33, respectively. In contrast, liquid-liquid phase  
24 separation (LLPS) did not occur in the high O:C system of glycerol/AS, which had an O:C of 1.00. Additionally, the  
25 morphology of 38 out of the 40 aerosol particles that underwent LLPS was observed to be a core-shell. Our findings provide  
26 a comprehensive understanding of the pH-dependent LLPS in individual suspended aerosol droplets and pave the way for  
27 future research on phase separation of atmospheric aerosol particles.

## 28 1 Introduction

29 Atmospheric aerosol particles can directly and indirectly impact climate by absorbing and scattering light and acting as cloud  
30 condensation nuclei (Rosenfeld et al., 2014). Particle morphology is a critical factor influencing the physiochemical properties



31 of aerosols such as their optical properties, chemistry, and nucleation processes (Freedman et al., 2009; Corral Arroyo et al.,  
32 2022; Cosman et al., 2008; Lam et al., 2021; Petters and Kreidenweis, 2007; Mikhailov et al., 2021). Morphology can be  
33 broadly categorized into single-phase homogeneous morphology and phase separation morphology (Gorkowski et al., 2020),  
34 based on the phase state of the particle. For droplets with a phase separation morphology, the two main equilibrium  
35 morphologies are a fully engulfed (core-shell) structure and a partially engulfed structure (Freedman, 2020). Droplets can  
36 undergo phase transition processes and thus the morphology would be changed. The composition and mass of inorganic and  
37 organic components impact the phase transition characteristics of a particle. With a decrease of particle water content, a  
38 transition occurs from single homogenous liquid phase to two separated liquid phases, which is known as liquid-liquid phase  
39 separation (LLPS). The relative humidity (RH) when the LLPS occurs is defined as separation relative humidity (SRH). The  
40 reverse process, in which two liquid phases mix into a single homogenous liquid phase, is referred to as liquid-liquid phase  
41 mixing and the corresponding RH is the mixing RH (MRH; Gorkowski et al., 2017).

42 The phenomenon of LLPS has garnered considerable attention from the atmospheric research community due to its potential  
43 role in affecting the physiochemical properties of atmospheric aerosols. Song et al. (2012) using optical microscopy studied  
44 the relationship between LLPS and the oxygen-to-carbon ratio (O:C) and discovered that LLPS was consistently observed  
45 when  $O:C < 0.56$ , while it was never observed when  $O:C > 0.80$ . For  $O:C$  between 0.56 and 0.80, the occurrence of LLPS  
46 was influenced by the types of organic functional groups. Gorkowski et al. (2020) utilized experimental results of previous  
47 studies on LLPS and morphology, observing a general trend in morphology from partially engulfed to core shell and finally  
48 homogeneous as oxidation increased. More recently, Kucinski et al. (2021) found that submicrometer-sized aerosol particles  
49 had a lower SRH compared to micrometer-sized droplets. Meanwhile, Stewart et al. (2015) employed aerosol optical tweezer  
50 (AOT) to investigate the morphologies of aqueous droplets. They found in the polyethylene glycol (PEG)/ammonium sulfate  
51 (AS) system, droplets formed predominately core-shell particles when the AS content was high and partially engulfed when  
52 the PEG content was high.

53 One factor that could influence the phase transitions of aerosol particles is the aerosol pH. The pH values for misty cloud and  
54 fog droplets generally range between 2 and 7, whereas continental and marine aerosol particles exhibit a wider range of pH  
55 values, from -1 to 5 and 0 to 8, respectively (Pye et al., 2020; Angle et al., 2021; Weber et al., 2016; Tilgner et al., 2021; Zheng  
56 et al., 2020). Meanwhile, aerosol pH is size-dependent, with the fine mode showing lower 1–4 pH units than the coarse mode  
57 (Fang et al., 2017; Young et al., 2013; Guo et al., 2017). Losey et al. (2018) measured the RH of phase transitions using optical  
58 microscopy and discovered that for low-pH aerosol particles ( $\leq 0.35$ ), phase separation may be hindered by the addition of  
59 sulfuric acid. However, it should be noted that the study utilized substrate-deposited droplets, which means the effect of the  
60 contact of the coverslip on droplet morphology cannot be disregarded. More recently, Tong et al. (2022) investigated the effect  
61 of acidity on phase separation in single suspended microdroplets using AOT. Their results showed that the pH can affect the  
62 miscibility of the mixture and high acidity results in a reduced SRH of 1,2,6-hexanetriol. Nevertheless, parallel experiments  
63 in this study were not conducted to accurately determine the uncertainty of the measurements.



64 Our aim with this work is to gain a comprehensive understanding of the influence of pH on phase transitions in suspended  
65 droplets. To that end, we investigate pH-dependent SRH and MRH, as well as morphologies of aqueous droplets using AOT,  
66 meanwhile discussed the effect of O:C on phase separation behavior. Compared to substrate-based measurement techniques,  
67 AOT can suspend droplets without any substrate contact, providing a more realistic simulation of the behavior of aerosols in  
68 the atmosphere. (Wang et al., 2021; Cui et al., 2021; Redding et al., 2015; Gong et al., 2018; Rafferty et al., 2023). We measured  
69 droplets containing AS and a range of organic compounds with varying O:C. We discuss how our findings provide insight into  
70 the mechanisms behind pH-dependent phase transitions in levitated droplets, along with the implications for fields such as  
71 climate science. Overall, our study highlights the importance of considering pH as a key factor in the phase transition behavior  
72 of micron-sized droplets and underscores the need for further research to fully understand the complex interactions between  
73 pH and phase transitions in these atmospherically relevant systems.

## 74 **2 Methods**

### 75 **2.1 Aerosol generation**

76 Four organics components: glycerol (GL), 3-methylglutaric acid (3-MGA), 1,2,6-hexanetriol (HEXT), and 2,5-hexanediol  
77 (HEXD), were chosen because they are commonly-used secondary organic aerosol (SOA) proxies (Lam et al., 2021;  
78 Gorkowski et al., 2020). O:C of the selected chemicals varied from 1 to 0.33 (**Table 1**), which is similar to the real  
79 atmospheric SOA (Canagaratna et al., 2015; Mahrt et al., 2021). AS was chosen as the inorganic salt component due to its  
80 widespread occurrence in the atmospheric environment. All concentrations of organics and AS in the mother solutions were  
81 50 g/L. The pure organic and inorganic components were dissolved in ultrapure water (Millipore, resistivity of 18.2M $\Omega$ ) to  
82 create solutions with OIR of 1:1. The pH of each solution was measured using a pH meter (Mettler Toledo Instruments Co.,  
83 Ltd., Shanghai, China), and adjusted as necessary using either concentrated sulfuric acid (SA) or sodium hydroxide (NaOH)  
84 solution (5.29 mol/L). Four to six solutions were prepared for each system with pH values ranging from 0.48 to 6.53. The  
85 purity and supplier of the compounds used in this study were summarized in **Table S1**.

86



**Table 1.** Information of the solutions used to generate aerosol droplets.

Solution ID	Organic component	O:C ratio	pH
GL	glycerol	1.00	5.24±0.01
3-MGA-I	3-methylglutaric acid	0.67	0.48±0.01
3-MGA-II			1.19±0.01
3-MGA-III			2.70±0.01
3-MGA-IV			3.70±0.01
3-MGA-V			5.21±0.02
3-MGA-VI			6.53±0.02
HEXT-I	1,2,6-hexanetriol	0.50	0.92±0.01
HEXT-II			2.02±0.01
HEXT-III			3.14±0.01
HEXT-IV			5.11±0.02
HEXD-I	2,5-hexanediol	0.33	1.39±0.01
HEXD-II			2.03±0.01
HEXD-III			2.71±0.01
HEXD-IV			3.13±0.01
HEXD-V			5.01±0.01

87

88

## 89 2.2 Experimental setup

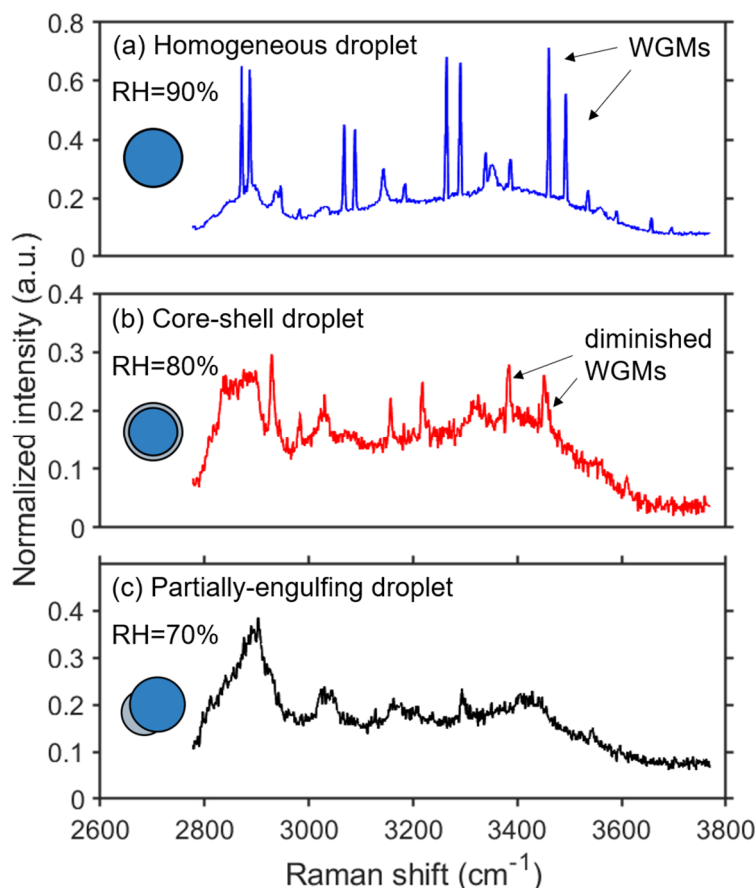
90 A schematic illustration of the experimental setup is presented in **Fig. S1**. The aerosol optical tweezer system consists of a  
 91 custom-made levitation chamber that integrates the optical trapping system, the illumination and imaging system, and the  
 92 aerosol generation system. A 532 nm (Opus 532-2W) laser was used to create an optical trap with a 100x oil immersion  
 93 objective (Olympus, UPLFLN100XO, NA 1.30) pressed against a glass coverslip (Nest, thickness 160-190 μm). The  
 94 illumination and imaging system includes a 450 nm LED (Daheng Optics, GCI060404) and a camera (Thorlabs, CS165CU/M)  
 95 to illuminate and image the particle. Two low pass filters (Andover, 500FL07-25) were used in front of the camera lens to  
 96 remove the influence of back scattered light of the 532 nm laser to photograph clear image of the particle. The Raman scattered  
 97 light passed through two 50:50 beam splitters (CVI Laser Optics, BTF-VIS-50-2501M-C) and a notch filter (Semrock, NFD01-  
 98 532-25x36) and was focused into the Raman spectrograph. A spectrograph (ZOLIX, Omni-λ5004i) is used to measure the  
 99 Stokes shifted Raman spectrum. A 20 μm entrance slit width and 1200 groove/mm diffraction grating with blaze wavelength  
 100 of 500 nm were used to achieve a spectral resolution of 0.021 nm. The wavelength position of spectrograph was calibrated  
 101 with Hg-laser. The Raman scattered light was recorded every 4 second with range of 624.24-665.40 nm.



102 As droplets are introduced continuously into the chamber from a medical nebulizer (LANDWIND, PN100), smaller droplets  
103 undergo a process of collision and coalescence, leading to the formation of larger droplets that can be readily trapped near the  
104 focal point of the laser. In most cases, droplets can be successfully captured within 30 s after the introduction of an aerosol  
105 plume into the cell. Air with relative humidity (RH) of 100% and 0% were mixed to produce wet air with a desired RH. The  
106 flow rates of the humidified and dry air streams were regulated by mass flow controllers (MFCs, Tianjin Gastool Instruments  
107 Co., Ltd., Tianjin, China, GT130D), with a combined flow rate of 0.3 L/min in total. Two humidity sensors (Sensirion, SHT85)  
108 were utilized, with a precision of  $\pm 1.5\%$ . Since the sensor located behind the chamber was positioned in close proximity ( $\sim 80$   
109 mm) to the droplet, its observed values were used as a surrogate for measuring the RH inside the chamber. The RH values  
110 were reduced in increments of 5% every 30 minutes (Tong et al., 2022; Stewart et al., 2015) until droplet phase separation  
111 occurred. The measured values of RH given by the sensors were used as the phase separation RH. Subsequently, the RH level  
112 was set to 100%, to investigate the phase mixing of the droplets. The entire experiment was repeated 1~4 times for each system.

### 113 **2.3 Determination of phase transitions**

114 When a transparent or weakly absorbing spherical particle is trapped, it can behave as a high-quality factor optical cavity that  
115 supports sharp optical resonances, resulting in cavity-enhanced Raman scattering. These resonances can be observed as peaks  
116 in the Raman spectrum of a particle and are often referred to as whispering gallery modes (WGMs). In principle, particle  
117 morphology can be deduced from the WGMs, as inhomogeneities in the refractive index can disrupt the circulation of the  
118 WGMs (Lin et al., 1992; Mitchem et al., 2006). Raman spectra measurements of single droplets in various morphological  
119 states are presented in **Figure 1**. When the droplet was in a homogeneous phase morphology, the droplet acted as a high-  
120 quality microcavity and sharp WGM peaks overlapped with the spontaneous Raman spectrum (**Fig. 1a**). When the droplet was  
121 in a state of a core-shell structure, observed WGMs were clearly diminished in measured spectra (**Fig. 1b**). The origin of the  
122 damping of the WGMs is the radial homogeneity that is present when the particle is separated into a hydrophilic core and a  
123 hydrophobic shell. As a result, when fitting the Raman spectra with the Mie scattering model for homogeneous droplets, the  
124 error in the best-fits greatly increase. Examination of the retrieved radius and refractive index reveals a clear break with fits  
125 for that of a homogeneous sphere. Therefore, the point at which a significant break in particle size and refractive index occurred  
126 can be used as the point at which core-shell phase separation occurs. As illustrated in **Fig. 1c**, when the droplet was partially-  
127 engulfed and non-spherical, WGM peaks in the spectrum are absent (Reid et al., 2011). Overall, the results of this analysis  
128 demonstrate the dynamic changes in the Raman spectra of single droplets as they undergo morphological transitions (Sullivan  
129 et al., 2020; Stewart et al., 2015; Tong et al., 2022).



130

131 **Figure 1.** Raman spectra of 3-MGA-II microdroplets: (a) a homogenous droplet (RH = 90%); (b) a core-shell droplet (RH =  
132 80%); (c) a partially-engulfed droplet (RH=70%). The WGMs are marked by black arrows.

133

134 The peak finding method used in this study is based on the ipeak code developed by O'Haver (2022). In short, the code first  
135 smooths the first derivative of the signal and identified downward-going zero-crossings that met a certain predetermined  
136 minimum slope and amplitude threshold. By adjusting the corresponding parameters, it is possible to accurately detect the  
137 desired peaks. The algorithm used to fit WGM peaks in spectra from homogenous spheres in this study was proposed by  
138 Preston and Reid (2013) and Preston and Reid (2015). The algorithm compares observed peak positions to expected positions  
139 calculated using a resonance condition from Mie theory. Error is minimized by varying particle size and refractive index (i.e.  
140 the parameters of best-fit). The method has been demonstrated to provide a rapid determination of the fitted radius and  
141 refractive index with an accuracy of  $\pm 2$  nm and  $\pm 0.0005$ , respectively. All of the Raman spectra used in this study were  
142 normalized by the area below the spontaneous Raman signals.

143

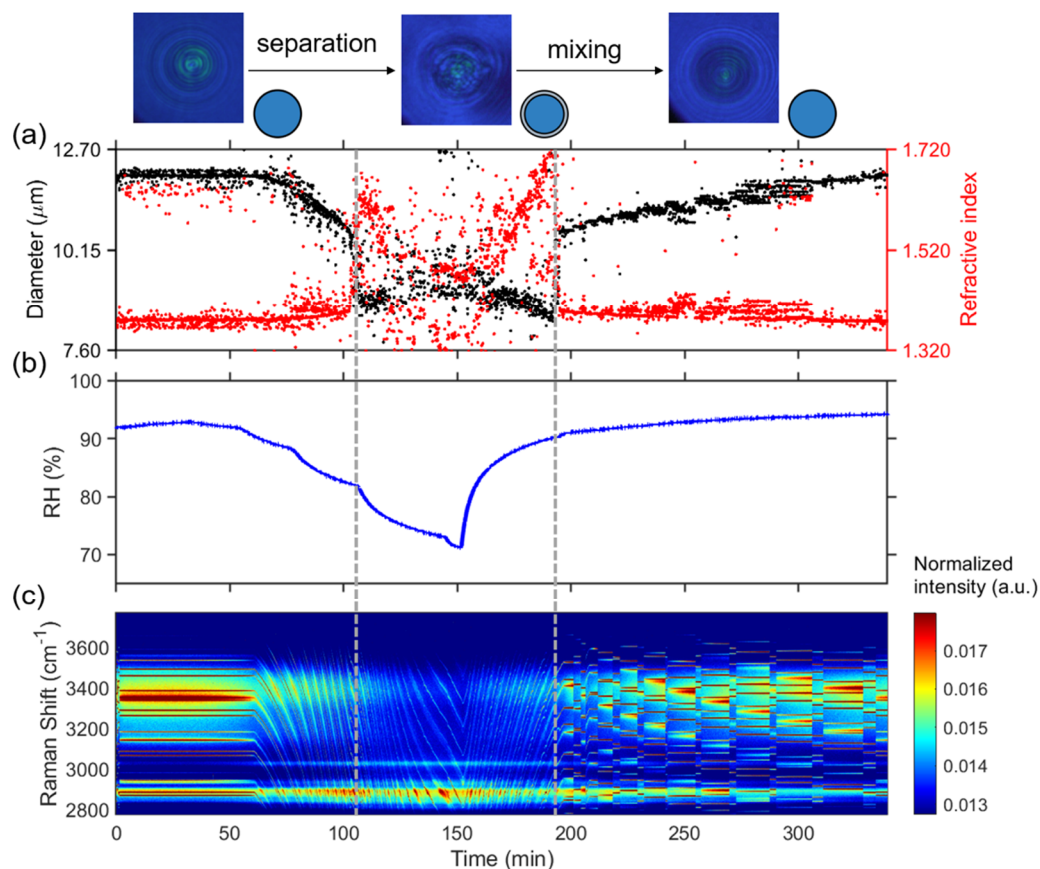


144 **3 Results and discussion**

145 **3.1 Phase behaviors of droplets mixed SOA proxy with AS**

146 **Figure 2** presents the results of time-resolved Raman spectra of aerosol droplets produced from a 3-MGA-II solution under  
147 continuously varying RH, as well as the corresponding particle size and refractive index values. To enable temperature and  
148 RH to stabilize, the chamber was conditioned with airflow for 50 minutes after trapping a particle. During the dehumidification  
149 process, the particle diameter decreased from 11.85  $\mu\text{m}$  to 9.03  $\mu\text{m}$  and the refractive index increased from 1.379 to 1.475  
150 when RH decreased from 93.0% to 70.0%. The particle size and water content decreased with RH due to the equilibrium  
151 partitioning of water molecules between vapor and droplets. Meanwhile, the refractive index of the droplets gradually increased  
152 as the water content decreases. When LLPS occurred, the droplets changed from a symmetrical homogeneous phase to an  
153 asymmetrical partially engulfed structure which led to the disappearance of the WGMs, or the formation of a core-shell  
154 structure. As RH in the reaction chamber was reduced, the LLPS was initiated, marked by the variations of the WGM signal  
155 (See **Fig. 1b**). This was achieved by reducing setting RH (setting values) by 5% at 30-minute intervals until the organic phase  
156 separated from the water-rich phase and then continuing decreasing RH by 10%-15%. **Fig. 2a** illustrates how the fitting of the  
157 droplet diameter and the refractive index deteriorated as the shell develops, indicating phase separation. The refractive index's  
158 shift results from a significant change in the radial profile due to the formation of a core-shell structure. Additionally, the  
159 persistence of strong WGMs indicates that the morphology of the droplet remains spherical following LLPS and is core-shell.  
160 During the RH increased from 70% to 95%, the reappearance of the continuously shifting WGM signal is observed, suggesting  
161 that the inorganic phase has mixed with the organic phase, and droplet returned to a homogeneous phase. During the  
162 humidification process, there is an opposite trend observed in the particle size and refractive index of the droplet compared to  
163 the dehumidification process. In conclusion, the variations of the WGM signal can serve as a reliable indicator of the  
164 occurrence of liquid-liquid phase separation or mixing, and the RH at these points can be considered as the SRH or MRH,  
165 respectively. The observed phase transitions of droplets produced from HEXT-IV and HEXD-V solutions were shown in **Fig.**  
166 **S2** and **Fig. S3**, respectively.

167



168

169 **Figure 2.** Liquid-liquid phase separation and mixing of aqueous 3-MGA-II. Schematic diagram of phase states is on the top  
 170 of the figure. (a) Timescale of changes in droplet size and refractive index, determined from fitting the Raman shift positions  
 171 of the WGMs. (b) RH variation after the trapping chamber during the humidity changing process. (c) Time-resolved Raman  
 172 spectra. The cessation of the random motion of inclusions within the droplet and the resultant formation of a core-shell structure  
 173 are indicated by the grey dashed line on the left. The grey dashed line on the right serves as an indication of the point at which  
 174 the droplet morphology transitioned from a state of separated phases to a homogeneous phase. The Raman spectra at 53 min, 113  
 175 min, 130 min are shown in **Fig. 1(a), (b), (c)**, respectively. Fitting errors of the WGMs were presented in **Fig. S5**.

176

177 **Figure S2** presents the results of time-resolved Raman spectra of aerosol droplets produced from GL/AS solution under  
 178 continuously varying RH, as well as the corresponding particle diameter and refractive index values. At the start of the  
 179 experiment, the chamber RH was held at 93% for approximately 75 minutes. The spectrum during this period reveals a clear  
 180 bright trend, indicative of the presence of many WGMs in the newly captured droplets. As the chamber RH dropped to a  
 181 minimum value of 71.5% at around 200 minutes, the position of the WGMs in each spectral snapshot shifted continuously,  
 182 following the same trend as the chamber RH. This observation suggests that the droplet was homogeneous and that no phase





183 separation occurred in the experimental RH range. The phenomenon regarding the GL/AS system is consistent with the  
184 conclusion by Song et al. (2013) and Gorkowski et al. (2020).

### 185 3.2 Effect of pH on SRH and MRH of different systems

186 The SRH and MRH of aerosol droplets produced from 3-MGA-I~VI solution are shown in **Fig. 3a**. The SRH values were  
187 92.7%, 89.5%, 80.6%, 79.7%, 76.2% and 69.7% at pH of 6.53, 5.21, 3.70, 2.70, 1.19 and 0.48, respectively. This decrease in  
188 SRH was attributed to the salting out ability of ammonium sulfate that is weakened at lower pH, and thus hinders the ability  
189 of organic matter to precipitate out of the solution (Losey et al., 2018). The MRH values at pH 6.53, 5.21, 2.70, 1.19 and 0.48  
190 were 87.6%, 89.5%, 87.3%, 83.9% and 83.5%, respectively, and are generally higher than corresponding SRH, especially in  
191 the low pH range (<5.00). The hysteresis between SRH and MRH existed because the SRH process has an activation barrier  
192 while the MRH process does not, and lower RH is needed for the aerosol droplet to overcome the activation barrier to form  
193 two phases (Freedman, 2020). Similar results were also observed in HEXT/AS and HEXD/AS systems. Additionally, the pH-  
194 dependent SRHs obtained in this study were compared to those reported by Losey et al. (2018), as depicted in **Fig. 3a**. It is  
195 worth mentioned that the solute concentration used in our study (50g/L) is comparable to Losey et al. (2018) (5.0 wt%),  
196 allowing for meaningful comparison of results. Overall, the SRHs of 3-MGA obtained in this study was higher than the results  
197 of Losey et al. (2018). When the pH was lower than 3.70, in 3-MGA system, the present study followed a similar trend as the  
198 results of Losey et al. (2018), with the SRH decreasing as the pH decreased. However, when the pH was greater than 3.70, our  
199 study showed an opposite trend compared to the results of Losey et al. (2018). The observed discrepancy may be attributed to  
200 the different methodologies employed. The present study utilized an optical tweezer system to capture droplets of ~10 µm  
201 diameter and the results were obtained using a spectrometer, while Losey et al. (2018) allowed ~100 µm size droplets to settle  
202 on a hydrophobic surface and observed the samples using an optical microscope. Kucinski et al. (2019) reported that the  
203 particle size has a significant impact on the phase separation of micro-droplets. The spherical morphology and smaller size in  
204 this study enhances the Kelvin effect, resulting in higher possibilities of phase separation occurring within droplets. The  
205 difference in droplet size is significant and the droplets used in this study are more representative of real atmospheric particulate  
206 matter, whereas the droplet properties in Losey et al. (2018) may be influenced by the surface they came into contact with.  
207 Thus, the utilization of an optical tweezer system provides a more realistic simulation of the evolution of particulate matter in  
208 the atmosphere.

209 In addition to 3-MGA, we also studied two organic/AS systems to investigate how acidity affects SRH and MRH of aerosols  
210 of differing composition. These results are shown in **Fig. 3** and tabulated in **Table 2**. The data suggests that acidity did not  
211 have a noticeable effect on the MRH of the various systems. The pH of the HEXT/AS solution without the addition of any  
212 acid was 5.11, and sulfuric acid was utilized to adjust the pH to lower levels (3.14, 2.02 and 0.92). The SRH values of  
213 HEXT/AS system (O:C=0.50) decreased as the pH decreased, with values of 78.3%, 76.6%, 76.4% and 75.7% at pH values  
214 of 5.11, 3.14, 2.02 and 0.92, respectively. The trend is similar to the 3-MGA (O:C=0.67) system, and the reason why SRH



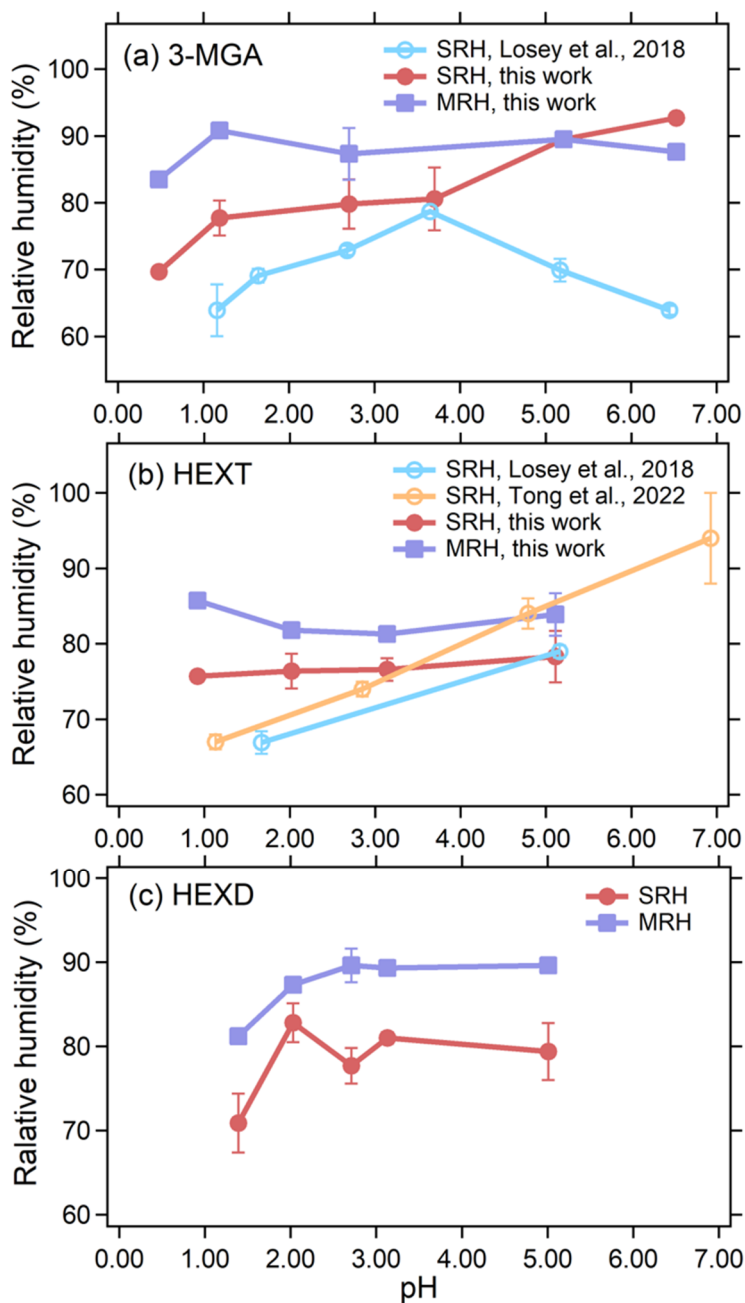
215 decreased may be due to the acid enhancing the miscibility of organic alcohols and inorganic substances, resulting in a greater  
216 difficulty in separating the hydrophobic phase from the water-rich phase (Tong et al., 2022). Still, we observed SRH was not  
217 strongly dependent on pH for HEXT/AS, compared to 3-MGA/AS system. This is likely due to the fact that organic alcohols  
218 have a large  $pK_a$  (e.g. the  $pK_a$  of HEXT is 14.3) and therefore exhibit minimal ionization in the pH range studied here (Wade  
219 and Simek, 2020). Additionally, the relative molecular interactions between alcohols and water are weaker than those of acids,  
220 leading to a weaker dependence of salting out ability of AS in the HEXT/AS system. The results of Losey et al. (2018) and  
221 Tong et al. (2022) were also depicted in **Fig. 3b**. Our results were higher than those of Losey et al. (2018), but the trend was  
222 similar. We attribute this discrepancy to a similar reason as that of the 3-MGA/AS system, which was previously discussed in  
223 this article. In contrast to the findings of Tong et al. (2022), our study observed a less pronounced trend in the values of SRH,  
224 and a narrower range in the distribution of SRH compared to literature values. The difference in OIR between this study (1:1)  
225 and Tong et al. (2022) (2:1) may account for the discrepancy in SRH. Previous studies (Ma et al., 2021; Stewart et al., 2015;  
226 Song et al., 2012) indicated that OIR differences could affect SRH, but SRH was not significantly dependent on OIR. For  
227 HEXD/AS (O:C=0.33) system, SRH decreases significantly when the pH is less than 2.00, while acidity had no significant  
228 effect on SRH when pH is greater than 2.00, with values of 79.4%, 81.0%, 77.7%, 82.8% and 70.9% at pH values of 5.01,  
229 3.13, 2.71, 2.03 and 1.39, respectively. This phenomenon was attributed to a mechanism similar to that observed in HEXT/AS.  
230 To our knowledge, this is the first investigation on the pH-dependent phase transition of HEXD/AS at the single particle level  
231 in a contact-free environment.

232 Our research suggests that in real atmospheric conditions where many ambient aerosol particles exhibit high acidity (Angle et  
233 al., 2021; Song et al., 2018; Liu et al., 2019; Li et al., 2022), droplets encounter heightened impediments to phase separation  
234 and tend to display a homogeneous structure. Although we used bulk solution pH as an indicator of pH at droplet phase  
235 transition, previous studies (Craig et al., 2018; Coddens et al., 2019; Li et al., 2023) have shown that the pH deviation between  
236 single microdroplet measurements and bulk solution measurements is small. Therefore, we consider our results valid. However,  
237 this study focused on volatile organics and was conducted over a relatively long period, which may have affected our results.  
238 Nevertheless, since the droplets studied here were relatively large (diameter 6-14  $\mu\text{m}$ ), we believe that any such influence can  
239 be neglected.

240



241



242 **Figure 3.** SRHs and MRHs as a function of pH for (a) 3-MGA/AS system, (b) HEXT/AS system, (c) HEXD/AS system.  
243 Hollow circles represent data from Losey et al. (2018) and Tong et al. (2022). The error bars of SRHs and MRHs are derived  
244 from multiple measurements.  
245



246 **Table 2.** SRH information for each pH studied as well as initial diameter, separation diameter (SD), separation relative index  
 247 (SRI), MRH, mixing diameter (MD), and mixing relative index (MRI) data.

3-MGA/AS system (O:C=0.67)							
Initial pH	Initial Diameter(nm)	SRH (%)	SD (nm)	SRI ( $\lambda=650\text{nm}$ )	MRH (%)	MD (nm)	MRI ( $\lambda=650\text{nm}$ )
0.48	10.97±1.57	69.7±0.2	7.23±1.72	1.515±0.086	83.5	6.82	1.540
1.19	11.23±1.20	77.7±2.6	8.68±2.38	1.454±0.100	90.8±0.2	9.08±1.64	1.394±0.009
2.70	10.60±2.28	79.8±3.7	7.83±1.71	1.480±0.112	87.3±3.9	7.86±1.63	1.483±0.118
3.70	10.87±1.87	80.6±4.7	7.24±1.00	1.491±0.088			
5.21	11.65±1.80	89.5±0.4	8.88±0.20	1.369±0.007	89.5	7.89	1.381
6.53	13.79	92.7	10.10	1.262	87.6	7.85	1.387
HEXT/AS system (O:C=0.50)							
0.92	14.04	75.7	10.58	1.438	85.7	10.83	1.420
2.02	12.88±1.0	76.4±2.3	9.09±0.46	1.409±0.007	81.8	9.34	1.410
3.14	12.31±0.8	76.6±1.5	9.01±0.47	1.408±0.002	81.3	9.04	1.409
5.11	13.53±0.4	78.3±3.4	9.15±0.35	1.396±0.014	83.9±2.8	9.04±0.73	1.412
HEXD/AS system (O:C=0.33)							
1.39	11.48±0.78	70.9±3.5	7.45±0.77	1.406±0.008	81.2	7.93	1.406
2.03	10.54±0.57	82.8±2.3	7.90±0.99	1.382±0.007	87.3	8.83	1.392
2.71	14.55±1.36	77.7±2.1	8.30±0.28	1.391±0.009	89.6±2.0	8.53±0.32	1.388±0.010
3.13	11.02±0.62	81.0±0.7	8.97±0.22	1.384±0.016	89.3	9.14	1.384
5.01	12.22±2.73	79.4±3.4	8.33±0.40	1.384±0.019	89.6±0.1	8.38±0.54	1.390±0.004

248

249 **3.3 Effect of O:C on phase separation behavior in different systems**

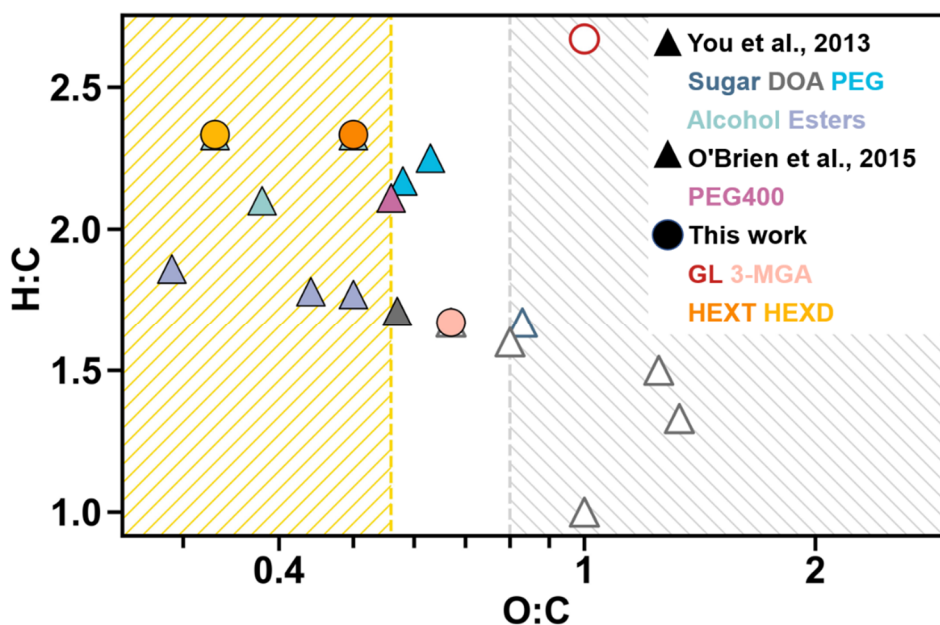
250 The phase separation behavior of organic aerosol particles is strongly influenced by their O:C. As shown in **Fig. 4**, our findings,  
 251 as well as those from previous studies (You et al., 2013; O'Brien et al., 2015), indicated that there is no correlation between  
 252 the occurrence of LLPS and the hydrogen-to-carbon (H:C) ratios of the organics, which is consistent with results in previous  
 253 findings (Bertram et al., 2011; Song et al., 2012). However, a clear trend was observed between LLPS occurrence and the O:C  
 254 of the organic components. We observed that droplets of 3-MGA/AS, HEXT/AS and HEXD/AS systems with O:C between  
 255 0.33 and 0.67 undergo LLPS. With the decrease of water content in the droplets, two distinct phases were formed: an organic-  
 256 rich phase and a salt-rich aqueous phase, under both acidic and neutral conditions. By contrast, no LLPS occurred in the GL/AS  
 257 system, as shown in **Fig. S2**. In general, particles with low O:C are more prone to undergo LLPS. This observation is consistent  
 258 with the findings of Song et al. (2012) who reported that LLPS was never observed when  $O:C > 0.80$  and always observed  
 259 when  $O:C < 0.56$ .

260 As shown in **Fig. 2** and **Table S2**, for most spectra, WGMs remained after LLPS occurred for droplets of 3-MGA/AS. This  
 261 phenomenon indicated that the droplets undergo LLPS with a core-shell morphology in most conditions, which is consistent



262 with the prediction of Gorkowski et al. (2020). Meanwhile, morphology of phase-separated droplets containing either HEXT  
 263 or HEXD were also core-shell shape mostly, as depicted in **Figure S3/S4** and **Table S3/S4**. It is attributed to the lower  
 264 interfacial tension observed at higher O:C, leading to higher possibility condition for forming core-shell shaped droplets  
 265 (Gorkowski et al., 2020). These findings support the idea that the O:C plays a crucial role in determining the morphology of  
 266 phase-separated particles in organic/inorganic mixed aerosols.

267



268

269 **Figure 4.** Van Krevelen Diagram for the mixed organic/AS particles: Solid symbols indicate that LLPS was observed, while  
 270 hollow symbols indicate that LLPS was not observed. Solid triangles represent dicarboxylic acids (DOA, including malonic  
 271 acid, malic acid, maleic acid, glutaric acid and diethylmalonic acid), sugars (levoglucosan), esters (including diethyl sebacate,  
 272 suberic acid monomethyl ester and poly diacrylate), alcohols (including 2,5-hexanediol, propylene glycol and 1,2,6-  
 273 hexanetriol), PEG (including PEG200 and PEG300) obtained from You et al. (2013), and AS-PEG400 obtained from O'Brien  
 274 et al. (2015).

275 **4 Conclusion**

276 The aim of this study was to investigate the effect of pH and O:C on phase transition behavior of levitated particles using the  
 277 AOT. Our results show that across aerosol pH in atmospheric condition, the presence of sulfuric acid inhibited the LLPS of  
 278 aerosol droplets that contained organics (3-MGA, HEXT, HEXD) and AS. Additionally, the MRHs were found to be higher  
 279 than the SRHs. The O:C of phase-separating systems is 0.67, 0.50, 0.33, and by contrast, LLPS of the high O:C system (GL,



280 O:C=1.00) did not occur. Meanwhile, the morphology of levitated aerosol particles was studied and we found that 38 out of  
281 40 droplets that underwent LLPS for a core-shell structure. The results presented here provide new insights into the behavior  
282 of different types of aerosol droplets, and the findings have important implications for our understanding of physical and  
283 chemical processes that occur in the atmosphere. It is anticipated that future studies will be carried out to examine the OIR-  
284 dependent phase separation in real acidified ambient aerosols. Such research will provide insights into the morphological  
285 characteristics of real aerosols and the ways in which these characteristics influence important properties such as  
286 hygroscopicity and homogenous chemistry. Such information will be helpful in furthering our understanding of the impacts of  
287 ambient aerosols on the environment and human health.

288 Additionally, in-situ measurement or pH estimation methods, such as the real-time AOT analysis in microdroplets reported  
289 by Boyer et al. (2020) could be combined with SRH measurements for a more accurate and comprehensive analysis.  
290 Furthermore, our study used a surrogate for SOA instead of in situ measurements of real SOA, which can be addressed in  
291 future work using SOA generated from a smog chamber or real SOA precursors and oxidized species.

292

293 **Data availability.** The data used in this paper can be obtained from the corresponding author upon request.

294 **Author contributions.** YC built the instrument, performed the experiments, analyzed the data, plotted the figures, and wrote  
295 the original draft. XP conceptualized the study, contributed to instrumentation, data analysis, discussion, and reviewed the  
296 manuscript. HL and CX contributed to the instrumentation and discussion. YM contributed to the experiments and discussion.  
297 ZX, FZ contributed to the discussion and manuscript review. TCP contributed to data analysis and manuscript review. ZW  
298 administrated the project, conceptualized the study, reviewed the manuscript, and contributed to funding acquisition.

299 **Competing interests.** The contact author has declared that none of the authors has any competing interests.

300 **Disclaimer.** Publisher's note: Copernicus Publications remains neutral with regard to jurisdictional claims in published maps  
301 and institutional affiliations.

302 **Financial support.** This research has been supported by the National Natural Science Foundation of China (grant nos.  
303 91844301, 42005087, and 42005086), Key Research and Development Program of Zhejiang Province (grant nos. 2021C03165,  
304 2022C03084), and the Fundamental Research Funds for the Central Universities (grant no. 2018QNA6008).

## 305 References

- 306 Rosenfeld, D., Sherwood, S., Wood, R., and Donner, L.: Climate effects of aerosol-cloud interactions, *Science*, 343, 379-380,  
307 <https://doi.org/10.1126/science.1247490>, 2014.
- 308 Freedman, M. A., Hasenkopf, C. A., Beaver, M. R., and Tolbert, M. A.: Optical properties of internally mixed aerosol particles  
309 composed of dicarboxylic acids and ammonium sulfate, *J. Phys. Chem. A*, 113, 13584-13592,  
310 <https://doi.org/10.1021/jp906240y>, 2009.
- 311 Corral Arroyo, P., David, G., Alpert, P. A., Parmentier, E. A., Ammann, M., and Signorell, R.: Amplification of light within  
312 aerosol particles accelerates in-particle photochemistry, *Science*, 376, 293-296, <https://doi.org/10.1126/science.abm7915>,  
313 2022.



- 314 Cosman, L. M., Knopf, D. A., and Bertram, A. K.: N<sub>2</sub>O<sub>5</sub> reactive uptake on aqueous sulfuric acid solutions coated with  
315 branched and straight-chain insoluble organic surfactants, *J. Phys. Chem. A*, 112, 2386, <https://doi.org/10.1021/jp710685r>,  
316 2008.
- 317 Lam, H. K., Xu, R., Choczynski, J., Davies, J. F., Ham, D., Song, M., Zuend, A., Li, W., Tse, Y. L. S., and Chan, M. N.:  
318 Effects of liquid–liquid phase separation and relative humidity on the heterogeneous OH oxidation of inorganic–organic  
319 aerosols: insights from methylglutaric acid and ammonium sulfate particles, *Atmos. Chem. Phys.*, 21, 2053–2066,  
320 <https://doi.org/10.5194/acp-21-2053-2021>, 2021.
- 321 Petters, M. D. and Kreidenweis, S. M.: A single parameter representation of hygroscopic growth and cloud condensation  
322 nucleus activity, *Atmos. Chem. Phys.*, 7, 1961–1971, <https://doi.org/10.5194/acp-7-1961-2007>, 2007.
- 323 Mikhailov, E. F., Pöhlker, M. L., Reinmuth-Selzle, K., Vlasenko, S. S., Krüger, O. O., Fröhlich-Nowoisky, J., Pöhlker, C.,  
324 Ivanova, O. A., Kiselev, A. A., Kremper, L. A., and Pöschl, U.: Water uptake of subpollen aerosol particles: hygroscopic  
325 growth, cloud condensation nuclei activation, and liquid–liquid phase separation, *Atmos. Chem. Phys.*, 21, 6999–7022,  
326 <https://doi.org/10.5194/acp-21-6999-2021>, 2021.
- 327 Gorkowski, K., Donahue, N. M., and Sullivan, R. C.: Aerosol optical tweezers constrain the morphology evolution of liquid-  
328 liquid phase-separated atmospheric particles, *Chem*, 6, 204–220, <https://doi.org/10.1016/j.chempr.2019.10.018>, 2020.
- 329 Freedman, M. A.: Liquid-liquid phase separation in supermicrometer and submicrometer aerosol particles, *Acc. Chem. Res.*,  
330 53, 1102–1110, <https://doi.org/10.1021/acs.accounts.0c00093>, 2020.
- 331 Gorkowski, K., Donahue, N. M., and Sullivan, R. C.: Emulsified and liquid-liquid phase-separated states of alpha-pinene  
332 secondary organic aerosol determined using aerosol optical tweezers, *Environ. Sci. Technol.*, 51, 12154–12163,  
333 <https://doi.org/10.1021/acs.est.7b03250>, 2017.
- 334 Song, M., Marcolli, C., Krieger, U. K., Zuend, A., and Peter, T.: Liquid-liquid phase separation in aerosol particles: dependence  
335 on O:C, organic functionalities, and compositional complexity, *Geophys. Res. Lett.*, 39, L19801,  
336 <https://doi.org/10.1029/2012GL052807>, 2012.
- 337 Kucinski, T. M., Ott, E. E., and Freedman, M. A.: Dynamics of liquid-liquid phase separation in submicrometer aerosol, *J.*  
338 *Phys. Chem. A*, 125, 4446–4453, <https://doi.org/10.1021/acs.jpca.1c01985>, 2021.
- 339 Stewart, D. J., Cai, C., Naylor, J., Preston, T. C., Reid, J. P., Krieger, U. K., Marcolli, C., and Zhang, Y. H.: Liquid-liquid  
340 phase separation in mixed organic/inorganic single aqueous aerosol droplets, *J. Phys. Chem. A*, 119, 4177–4190,  
341 <https://doi.org/10.1021/acs.jpca.5b01658>, 2015.
- 342 Pye, H. O. T., Nenes, A., Alexander, B., Ault, A. P., Barth, M. C., Clegg, S. L., Collett, J. L., Jr., Fahey, K. M., Hennigan, C.  
343 J., Herrmann, H., Kanakidou, M., Kelly, J. T., Ku, I. T., McNeill, V. F., Riemer, N., Schaefer, T., Shi, G., Tilgner, A.,  
344 Walker, J. T., Wang, T., Weber, R., Xing, J., Zaveri, R. A., and Zuend, A.: The acidity of atmospheric particles and clouds,  
345 *Atmos. Chem. Phys.*, 20, 4809–4888, <https://doi.org/10.5194/acp-20-4809-2020>, 2020.
- 346 Angle, K. J., Crocker, D. R., Simpson, R. M. C., Mayer, K. J., Garofalo, L. A., Moore, A. N., Mora Garcia, S. L., Or, V. W.,  
347 Srinivasan, S., Farhan, M., Sauer, J. S., Lee, C., Pothier, M. A., Farmer, D. K., Martz, T. R., Bertram, T. H., Cappa, C.  
348 D., Prather, K. A., and Grassian, V. H.: Acidity across the interface from the ocean surface to sea spray aerosol, *Proc.*  
349 *Natl. Acad. Sci. U.S.A.*, 118, e2018397118, <https://doi.org/10.1073/pnas.2018397118>, 2021.
- 350 Weber, R. J., Guo, H. Y., Russell, A. G., and Nenes, A.: High aerosol acidity despite declining atmospheric sulfate  
351 concentrations over the past 15 years, *Nat. Geosci.*, 9, 282–285, <https://doi.org/10.1038/ngeo2665>, 2016.
- 352 Tilgner, A., Schaefer, T., Alexander, B., Barth, M., Collett, J. L., Fahey, K. M., Nenes, A., Pye, H. O. T., Herrmann, H., and  
353 McNeill, V. F.: Acidity and the multiphase chemistry of atmospheric aqueous particles and clouds, *Atmos. Chem. Phys.*,  
354 21, 13483–13536, <https://doi.org/10.5194/acp-21-13483-2021>, 2021.
- 355 Zheng, G., Su, H., Wang, S., Andreae, M., Pöschl, U., and Cheng, Y.: Multiphase buffer theory explains contrasts in  
356 atmospheric aerosol acidity, *Science*, 369, 1374–1377, <https://doi.org/10.1126/science.aba3719>, 2020.
- 357 Fang, T., Guo, H., Zeng, L., Verma, V., Nenes, A., and Weber, R. J.: Highly acidic ambient particles, soluble metals, and  
358 oxidative potential: a link between sulfate and aerosol toxicity, *Environ. Sci. Technol.*, 51, 2611–2620,  
359 <https://doi.org/10.1021/acs.est.6b06151>, 2017.
- 360 Young, A. H., Keene, W. C., Pszenny, A. A. P., Sander, R., Thornton, J. A., Riedel, T. P., and Maben, J. R.: Phase partitioning  
361 of soluble trace gases with size-resolved aerosols in near-surface continental air over northern Colorado, USA, during  
362 winter, *J. Geophys. Res.: Atmospheres*, 118, 9414–9427, <https://doi.org/10.1002/jgrd.50655>, 2013.



- 363 Guo, H., Liu, J., Froyd, K. D., Roberts, J. M., Veres, P. R., Hayes, P. L., Jimenez, J. L., Nenes, A., and Weber, R. J.: Fine  
364 particle pH and gas-particle phase partitioning of inorganic species in Pasadena, California, during the 2010 CalNex  
365 campaign, *Atmos. Chem. Phys.*, 17, 5703-5719, <https://doi.org/10.5194/acp-17-5703-2017>, 2017.
- 366 Losey, D. J., Ott, E. J. E., and Freedman, M. A.: Effects of high acidity on phase transitions of an organic aerosol, *J. Phys.*  
367 *Chem. A*, 122, 3819-3828, <https://doi.org/10.1021/acs.jpca.8b00399>, 2018.
- 368 Tong, Y. K., Meng, X. X. Y., Zhou, B., Sun, R., Wu, Z. J., Hu, M., and Ye, A. P.: Detecting the pH-dependent liquid-liquid  
369 phase separation of single levitated aerosol microdroplets via laser tweezers-Raman spectroscopy, *Front. Phys.*, 10,  
370 <https://doi.org/10.3389/fphy.2022.969921>, 2022.
- 371 Wang, M., Zheng, N., Zhao, D., Shang, J., and Zhu, T.: Using micro-Raman spectroscopy to investigate chemical composition,  
372 mixing states, and heterogeneous reactions of individual atmospheric particles, *Environ. Sci. Technol.*, 55, 10243-10254,  
373 <https://doi.org/10.1021/acs.est.1c01242>, 2021.
- 374 Cui, X., Tang, M., Wang, M., and Zhu, T.: Water as a probe for pH measurement in individual particles using micro-Raman  
375 spectroscopy, *Anal. Chim. Acta.*, 1186, 339089, <https://doi.org/10.1016/j.aca.2021.339089>, 2021.
- 376 Redding, B., Schwab, M. J., and Pan, Y. L.: Raman spectroscopy of optically trapped single biological micro-particles, *Sensors*,  
377 15, 19021-19046, <https://doi.org/10.3390/s150819021>, 2015.
- 378 Gong, Z. Y., Pan, Y. L., Videen, G., and Wang, C. J.: Optical trapping and manipulation of single particles in air: principles,  
379 technical details, and applications, *J. Quant. Spectrosc. Ra.*, 214, 94-119, <https://doi.org/10.1016/j.jqsrt.2018.04.027>,  
380 2018.
- 381 Rafferty, A., Vennes, B., Bain, A., and Preston, T. C.: Optical trapping and light scattering in atmospheric aerosol science,  
382 *Phys. Chem. Chem. Phys.*, 25, 7066-7089, <https://doi.org/10.1039/d2cp05301b>, 2023.
- 383 Canagaratna, M. R., Jimenez, J. L., Kroll, J. H., Chen, Q., Kessler, S. H., Massoli, P., Hildebrandt Ruiz, L., Fortner, E.,  
384 Williams, L. R., Wilson, K. R., Surratt, J. D., Donahue, N. M., Jayne, J. T., and Worsnop, D. R.: Elemental ratio  
385 measurements of organic compounds using aerosol mass spectrometry: characterization, improved calibration, and  
386 implications, *Atmos. Chem. Phys.*, 15, 253-272, <https://doi.org/10.5194/acp-15-253-2015>, 2015.
- 387 Mahrt, F., Newman, E., Huang, Y., Ammann, M., and Bertram, A. K.: Phase behavior of hydrocarbon-like primary organic  
388 aerosol and secondary organic aerosol proxies based on their elemental oxygen-to-carbon ratio, *Environ. Sci. Technol.*,  
389 55, 12202-12214, <https://doi.org/10.1021/acs.est.1c02697>, 2021.
- 390 Lin, H. B., Eversole, J. D., and Campillo, A. J.: Continuous-wave stimulated Raman scattering in microdroplets, *P. Opt. Lett.*,  
391 17, 828-830, <https://doi.org/10.1364/ol.17.000828>, 1992.
- 392 Mitchem, L., Buajaren, J., Ward, A. D., and Reid, J. P.: A strategy for characterizing the mixing state of immiscible aerosol  
393 components and the formation of multiphase aerosol particles through coagulation, *J. Phys. Chem. B*, 110, 13700-13703,  
394 <https://doi.org/10.1021/jp062874z>, 2006.
- 395 Reid, J. P., Dennis-Smith, B. J., Kwamena, N. O. A., Miles, R. E. H., Hanford, K. L., and Homer, C. J.: The morphology of  
396 aerosol particles consisting of hydrophobic and hydrophilic phases: hydrocarbons, alcohols and fatty acids as the  
397 hydrophobic component, *Phys. Chem. Chem. Phys.*, 13, 15559-15572, <https://doi.org/10.1039/c1cp21510h>, 2011.
- 398 Sullivan, R. C., Boyer-Chelmo, H., Gorkowski, K., and Beydoun, H.: Aerosol Optical Tweezers Elucidate the Chemistry,  
399 Acidity, Phase Separations, and Morphology of Atmospheric Microdroplets, *Acc. Chem. Res.*, 11, 2498-2509,  
400 <https://doi.org/10.1021/acs.accounts.0c00407>, 2020.
- 401 O'Haver, T. C.: A pragmatic introduction to signal processing with applications in scientific measurement, Kindle Direct  
402 Publishing, ISBN: 9798611266687, 2022.
- 403 Preston, T. C. and Reid, J. P.: Accurate and efficient determination of the radius, refractive index, and dispersion of weakly  
404 absorbing spherical particle using whispering gallery modes, *J. Opt. Soc. Am. B*, 30, 2113-2122,  
405 <https://doi.org/10.1364/JOSAB.30.002113>, 2013.
- 406 Preston, T. C. and Reid, J. P.: Determining the size and refractive index of microspheres using the mode assignments from  
407 Mie resonances, *J. Opt. Soc. Am. A*, 32, 2210-2217, <https://doi.org/10.1364/JOSAA.32.002210>, 2015.
- 408 Bertram, A. K., Martin, S. T., Hanna, S. J., Smith, M. L., Bodsworth, A., Chen, Q., Kuwata, M., Liu, A., You, Y., and Zorn,  
409 S. R.: Predicting the relative humidities of liquid-liquid phase separation, efflorescence, and deliquescence of mixed  
410 particles of ammonium sulfate, organic material, and water using the organic-to-sulfate mass ratio of the particle and the  
411 oxygen-to-carbon elemental ratio of the organic component, *Atmos. Chem. Phys.*, 11, 10995-11006,  
412 <https://doi.org/10.5194/acp-11-10995-2011>, 2011.





- 413 Boyer, H. C., Gorkowski, K., and Sullivan, R. C.: In situ pH measurements of individual levitated microdroplets using aerosol  
414 optical tweezers, *Anal. Chem.*, 92, 1089-1096, <https://doi.org/10.1021/acs.analchem.9b04152>, 2020.
- 415 Coddens, E. M., Angle, K. J., and Grassian, V. H.: Titration of aerosol pH through droplet coalescence, *J. Phys. Chem. Lett.*,  
416 10, 4476-4483, <https://doi.org/10.1021/acs.jpcclett.9b00757>, 2019.
- 417 Craig, R. L., Peterson, P. K., Nandy, L., Lei, Z., Hossain, M. A., Camarena, S., Dodson, R. A., Cook, R. D., Dutcher, C. S.,  
418 and Ault, A. P.: Direct Determination of Aerosol pH: Size-resolved measurements of submicrometer and supermicrometer  
419 aqueous particles, *Anal. Chem.*, 90, 11232-11239, <https://doi.org/10.1021/acs.analchem.8b00586>, 2018.
- 420 Kucinski, T. M., Dawson, J. N., and Freedman, M. A.: Size-Dependent Liquid-Liquid Phase Separation in Atmospherically  
421 Relevant Complex Systems, *J. Phys. Chem. Lett.*, 10, 6915-6920, <https://doi.org/10.1021/acs.jpcclett.9b02532>, 2019.
- 422 Li, M., Kan, Y., Su, H., Pöschl, U., Parekh, S. H., Bonn, M., and Cheng, Y. F.: Spatial homogeneity of pH in aerosol  
423 microdroplets, *Chem*, in press, <https://doi.org/10.1016/j.chempr.2023.02.019>, 2023.
- 424 Li, M., Su, H., Zheng, G., Kuhn, U., Kim, N., Li, G., Ma, N., Poschl, U., and Cheng, Y.: Aerosol pH and ion activities of  
425  $\text{HSO}_4^-$  and  $\text{SO}_4^{2-}$  in supersaturated single droplets, *Environ. Sci. Technol.*, <https://doi.org/10.1021/acs.est.2c01378>, 2022.
- 426 Liu, M., Huang, X., Song, Y., Tang, J., Cao, J., Zhang, X., Zhang, Q., Wang, S., Xu, T., Kang, L., Cai, X., Zhang, H., Yang,  
427 F., Wang, H., Yu, J. Z., Lau, A. K. H., He, L., Huang, X., Duan, L., Ding, A., Xue, L., Gao, J., Liu, B., and Zhu, T.:  
428 Ammonia emission control in China would mitigate haze pollution and nitrogen deposition, but worsen acid rain, *Proc.*  
429 *Natl. Acad. Sci. U. S. A.*, 116, 7760-7765, <https://doi.org/10.1073/pnas.1814880116>, 2019.
- 430 Ma, S. S., Chen, Z., Pang, S. F., and Zhang, Y. H.: Observations on hygroscopic growth and phase transitions of mixed 1, 2,  
431 6-hexanetriol/ $(\text{NH}_4)_2\text{SO}_4$  particles: investigation of the liquid-liquid phase separation (LLPS) dynamic process and  
432 mechanism and secondary LLPS during the dehumidification, *Atmos. Chem. Phys.*, 21, 9705-9717,  
433 <https://doi.org/10.5194/acp-21-9705-2021>, 2021.
- 434 O'Brien, R. E., Wang, B. B., Kelly, S. T., Lundt, N., You, Y., Bertram, A. K., Leone, S. R., Laskin, A., and Gilles, M. K.:  
435 Liquid-liquid phase separation in aerosol particles: imaging at the nanometer scale, *Environ. Sci. Technol.*, 49, 4995-  
436 5002, <https://doi.org/10.1021/acs.est.5b00062>, 2015.
- 437 Song, M. J., Marcolli, C., Krieger, U. K., Lienhard, D. M., and Peter, T.: Morphologies of mixed organic/inorganic/aqueous  
438 aerosol droplets, *Faraday Discuss.*, 165, 289-316, <https://doi.org/10.1039/c3fd00049d>, 2013.
- 439 Song, S., Gao, M., Xu, W., Shao, J., Shi, G., Wang, S., Wang, Y., Sun, Y., and McElroy, M. B.: Fine-particle pH for Beijing  
440 winter haze as inferred from different thermodynamic equilibrium models, *Atmos. Chem. Phys.*, 18, 7423-7438,  
441 <https://doi.org/10.5194/acp-18-7423-2018>, 2018.
- 442 Wade, L. G. and Simek, J. W.: Acidity of alcohols and phenols, in: *Organic Chemistry*,  
443 <https://chem.libretexts.org/@go/page/45234>, 2020.
- 444 You, Y., Renbaum-Wolff, L., and Bertram, A. K.: Liquid-liquid phase separation in particles containing organics mixed with  
445 ammonium sulfate, ammonium bisulfate, ammonium nitrate or sodium chloride, *Atmos. Chem. Phys.*, 13, 11723-11734,  
446 <https://doi.org/10.5194/acp-13-11723-2013>, 2013.